Liquefied Bleed for Stability and Efficiency of High Speed Inlets

Project WBS Number: 694478.02.93.02.13.52.22

Investigators: J. David Saunders and Dr. David Davis, NASA Glenn Research Center, Inlet and Nozzle Branch; Dr. Stephen J. Barsi and Dr. Matthew C. Deans, NASA Glenn Research Center, Propulsion and Propellants Branch; Lois J. Weir and Bobby W. Sanders, TechLand Research, Inc.

Purpose

Through Phase 1 Seedling Fund support, a novel concept entitled, "Liquefied Bleed for Stability and Efficiency of High Speed Inlets" was investigated. The purpose of this 1-year effort was to quantify the design parameters and benefits of the liquefied bleed (LB) concept. The potential payoff is enhanced system performance of inlets for high-speed aircraft. Elements of the task include:

1) development of a physical configuration with thermal balance sufficient to cool the bleed air
2) development of a scheme to capture, process, and prevent icing conditions of the liquefied bleed air
3) analysis for first-order effects of cooling on the outflow of the bleed air
4) measurement of the bleed air thermal state (temperature and liquefaction fraction)
5) measurement of the resulting core (propulsive flow path) boundary-layer flow quality

The Phase 1 Seedling Fund effort focused on the first three elements by assembling tools, conducting preliminary analyses, and preparing test plans.

Background

Bleed air has traditionally been used for mixed-compression inlets at moderate to high supersonic flight speeds for stability and improved performance (see Figure 1).

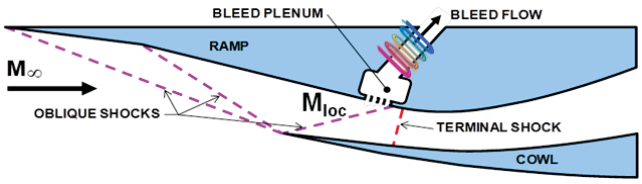

Figure 1. Mixed-compression inlet with bleed.

At higher speeds, however, the increased flight enthalpy causes extreme difficulties in using bleed. The bleed air drawn off of the propulsive flow path is at both high temperature and low pressure. Bleed ductwork becomes hot and large, and the bleed air produces increased vehicle drag when exhausted overboard. Therefore, uncooled bleed causes increased drag for supersonic propulsion and cannot effectively be used for hypersonic engine designs.

A photograph of a hypersonic research inlet referred to as the Combined-Cycle Engine Large Scale Inlet Mode Transition Experiment (CCE LIMX) is shown in Figure 2. This test article is a fully integrated Turbine-Based Combined-Cycle (TBCC) propulsion system and is currently undergoing testing in the NASA Glenn Research Center (GRC) 10- by 10-Foot Supersonic Wind Tunnel (10x10 SWT) at conditions approximating Mach 4 flight. Initial results from this test program are reported in References 1 and 2.

Figure 2. CCE LIMX installed in the NASA 10x10 SWT.

The series of pipes shown in the upper left of the photo are used to exhaust bleed air from the inlet. Sized to provide effective bleed at Mach 4 conditions, the frontal area of the bleed pipes are comparable to the engine ducts themselves.*

The above example serves to illustrate the difficulty of providing effective uncooled bleed at flight speeds of Mach 4 and higher. However, if the bleed air were to be cooled, the ductwork would become cooler and the size requirement would be reduced. Cooling of the bleed air would be provided by the cryogenic fuels that are required

*Note that this research inlet model did not have the bleed ducting sized to minimize frontal-area drag as would be done in a flight inlet design. Nevertheless, the photograph does qualitatively indicate the impact of bleed ducting.

by high-speed vehicles. The current research effort is focused on investigating the feasibility and effect of intensely cooling the bleed air to the point of liquefaction.

To date, prior studies have focused on quantifying the relationship between bleed flow rate and bleed duct pressure (Reference 3). A small subset of this research investigated the effect of wall cooling on boundary-layer development (Reference 4). The wall-cooling studies were not coupled to bleed flow extraction nor were the system-level benefits of liquefied bleed examined. The potential benefits of the cooling concepts include greatly reduced bleed duct sizing, reduced shock-wave/boundary-layer interaction extent, and oxidant storage for other phases of a flight mission. The concept will enable greatly improved performance and robustness of airbreathing propulsion and thereby enable new design options for high-speed flight.

Approach

For the Phase 1 effort, the technical approach addressed three key areas. First, the physical configuration and thermal balance requirements were analyzed. One of the issues considered was whether the air should be liquefied as it passes through the perforated bleed plate, or should it pass through a conventional bleed plate before entering a separate heat exchanger? The former may result in a more compact, lighter system, but the latter allows for the use of conventional bleed plates whose performance is well characterized, but may require their own cooling system at high Mach numbers. To keep the Phase 1 effort simple, the initial experiments were planned with a decoupled bleed plate and heat exchanger. Because of the slightly different (~57 °F) condensation temperatures for nitrogen and oxygen, the potential for the generation of liquid oxygen and the safety implications was also considered.

The second key area in Phase 1 was to conduct a simplified system study to understand the impact of a liquid bleed cryogenic subsystem on a high-speed vehicle. Estimates of weight and other cost/benefit trades were incorporated into a candidate vehicle concept.

Finally, in order to verify the liquid bleed concept, two proof-of-concept (POC) experiments were planned as part of the Phase 1 effort. These tests are anticipated to be conducted as part of a Phase 2 effort. The first experiment is a small-scale test with a limited number of bleed holes. This test is planned to be conducted in a cryogenics lab at NASA GRC where the infrastructure for handling cryogenic hydrogen and compatible systems is already in place. A small axisymmetric (3.0-in.-diameter) Mach 3 SWT has been designed and partially fabricated to support this test. The second test is a larger scale experiment that includes a complete bleed region with an impinging reflected shock wave as shown in Figure 3.

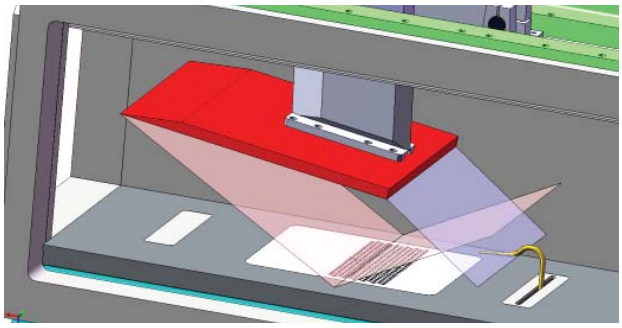

Figure 3. 1- by 1-Foot SWT with shock and bleed.

This test will be conducted in the NASA GRC 1- by 1-Foot SWT (1×1 SWT), which has a Mach number capability from M = 1.3 to 6.0 and has been used for bleed research in the past.

A cryogenic fluid cooling system would need to be added to the tunnel for the proposed cooled bleed experiment. One of the advantages of this facility is the large bleed plenum (Figure 4), which can easily accommodate the liquid-bleed subsystem.

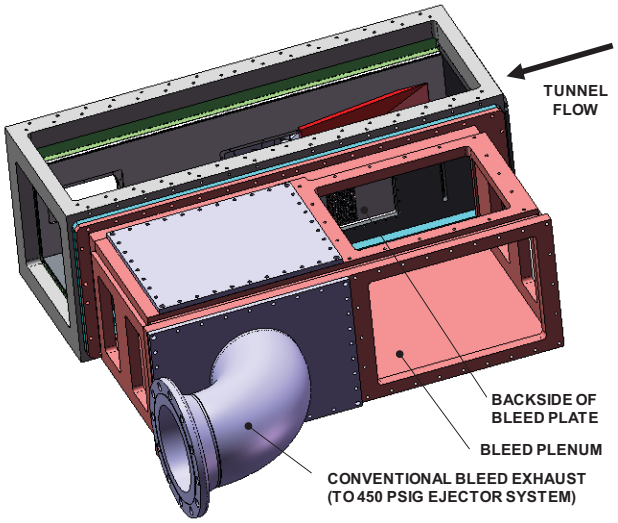

Figure 4. 1x1 SWT bleed plenum.

To address the significant challenge of test operations with cryogenic fluids, we are also investigating alternative facilities at the GRC Research Combustion Laboratory (RCL) as well as facilities outside NASA. As will be discussed, later, all these facility options would require modifications with cost impact.

Accomplishments

The Liquefied Bleed project progressed well through the technical feasibility and test planning phases. The following five accomplishments are detailed: 1) Feasibility, including thermal balance was confirmed, 2) Potential test facilities have been identified, 3) Mission analyses are encouraging, 4) Detailed test planning was completed, and 5) Test cost estimates were received.

Status of Research

Semi-monthly meetings were conducted since February 2013. These meetings coordinated the research analyses and plans between the researchers in two groups: supersonic inlets and the cryogenic propellants. Additional meetings occurred to gather cost information based on the test plans.

Figure 5 shows a previous small rocket test in the Altitude Combustion Stand (ACS), which is one of the facilities being considered for the small-scale POC test.

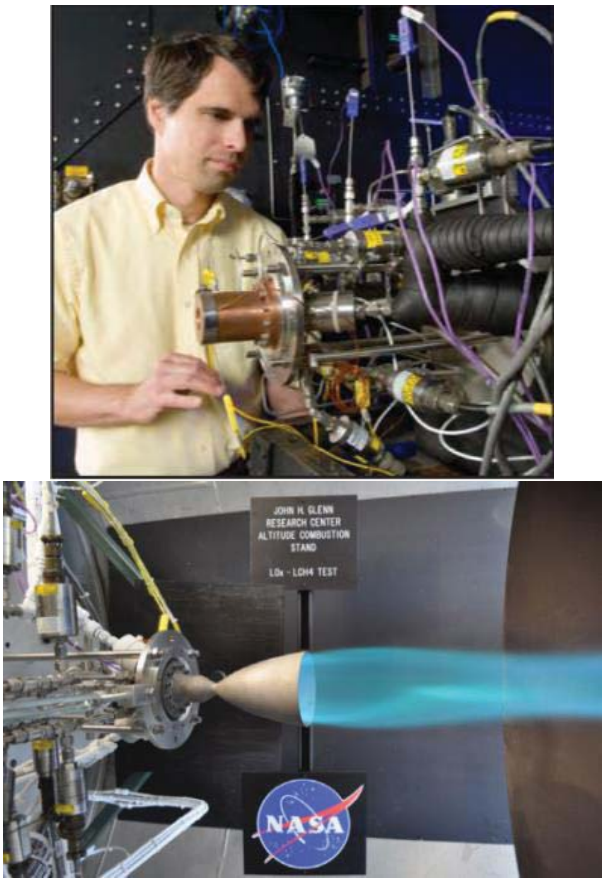

Figure 5. Cryogenic rocket testing at the ACS of the RCL.

Using experience from the TBCC mode transition inlet design, a range of bleed flow rates and fluid states were used to size the heat exchanger and facility equipment. From this bleed environment, an analysis was conducted to determine the thermodynamic effect of cryogenic cooling on the air density and liquefaction fraction. In Figure 6, plots of the bleed air's possible exit conditions as a function of hydrogen exit conditions are shown. In both cases, supercritical hydrogen is entering the heat exchanger at 225 psia and 36 R.

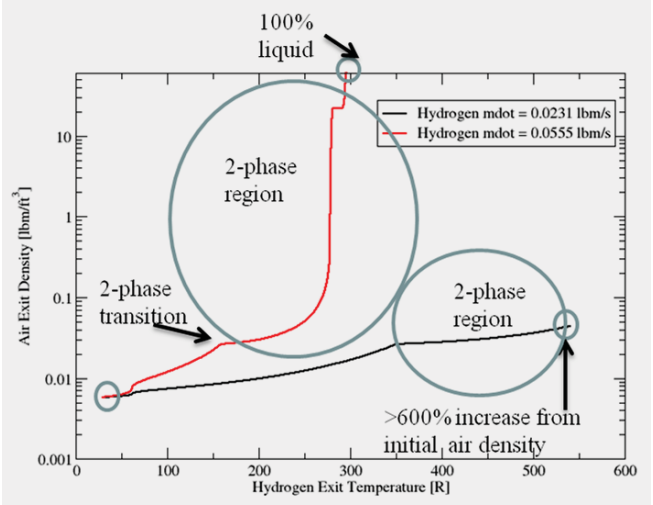

Figure 6. Bleed air exit conditions.

At a moderate liquid hydrogen flow rate, more than a 600% increase in bleed air density may be expected. If the hydrogen-to-bleed-air ratio is more aggressive, complete air liquefaction is possible. These results support concept feasibility. Heat exchanger sizing, design, and detailed test planning were based on these analyses. The thermal analysis effort is discussed in further detail in Appendix A.

The challenge of cryogenic hydrogen safety has led the research team to baseline some of GRC's propulsion and cryogenic fluid facilities in our test plans. Two test areas were considered, the ACS and Small Multi-propose Research Facility (SMiRF). Both are capable of testing cryogenic propellants. However, SMiRF is actively working with liquid hydrogen, whereas the fuel system for ACS is currently setup for liquid methane. The liquid hydrogen infrastructure was considered more valuable. Therefore, the SMiRF facility is preferred for the cryogenic testing.

As a consequence, the research team will plan for two possible test entries: 1) A POC test in a cryogenic (liquid hydrogen) facility. 2) Bleed testing in a larger wind tunnel, such as the 1×1 SWT (Refs. 5 and 6). These two entries could be conducted in parallel. For the POC cryotest, the research team elected to develop a small supersonic wind tunnel with a circular cross-section: diameter of 3 in. or a test section area of about 7 $in.^2$ A conceptual sketch of the proposed small supersonic wind tunnel and associated heat exchanger for bleed liquefaction is shown in Figure 7a. This heat exchanger design provides a large enough size to maintain minimum wall thickness for the fins and to install critical instrumentation.

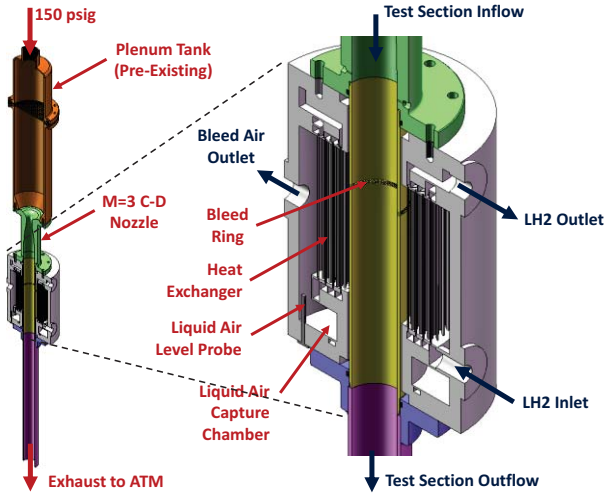

a) Sketch of the Liquefied Bleed experiment in SMiRF.

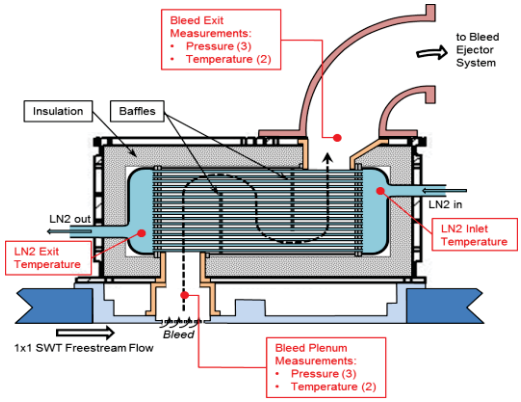

b) Bleed exhaust plenum with heat exchanger installed in the 1×1 SWT.

Figure 7. Heat exchanger installations in the two proposed test facilities for liquefied bleed.

Figure 7b depicts a cross section of the bleed exhaust plenum with a notional design of a heat exchanger installed in the 1×1 SWT. The sidewall of the wind tunnel test section is represented in blue at the bottom of the figure. The light blue piece is the (existing) tunnel sidewall bleed insert plate. Bleed airflow is removed from the freestream test section flow through the bleed insert plate. A plenum is mounted on top of the bleed pocket, capturing the removed airflow and delivering it into the heat exchanger. The notional heat exchanger is a basic "shell and tube two-pass straight-tube" heat exchanger.

For mission analysis, a FORTRAN-based simulation of a representative TBCC mission has been developed in order to capture the first-order effects of a LB system. The space-access mission that was modeled simulates an airbreathing TBCC-propelled first stage that could boost a second stage to Mach 7. The effect of a liquefied bleed system was assessed by assigning appropriate performance, weight fraction factors, and assumptions to find the resulting minimum take-off gross weight, TOGW. The liquefied bleed benefits are increased supersonic inlet recovery and reduced bleed drag and volume. The volume change accommodates a larger fuel fraction. For the preliminary analysis, the liquefied bleed air was assumed to be liquefied but not stored for later use. Other simplifying assumptions such as addressing thermal balance issues for the dual-mode ramjet or scramjet (DMRJ) flow path and optimal sizing of the TBCC aircraft can be investigated in the future. For the current analysis, baseline aircraft had a very large TOGW of 2×10^6 lbs. Figure 8 shows a preliminary result. More details are given in Appendix B.

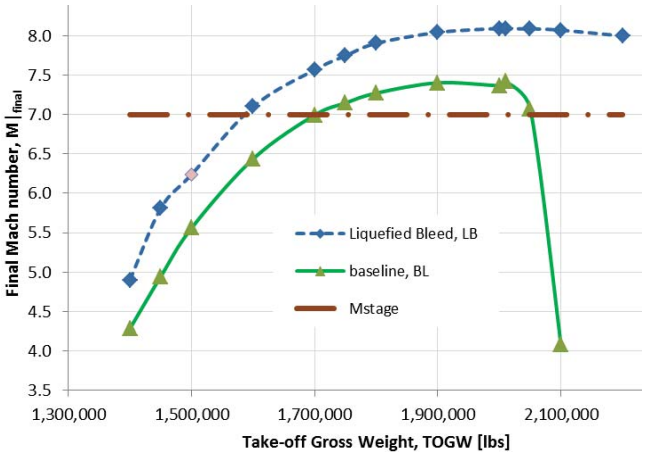

Figure 8. Results from mission analysis showing a 23% reduction in TOGW due to liquefied bleed.

This plot indicates that liquefied bleed could reduce TOGW by up to 23%. This benefit was accentuated by a pinch point at the turbine-to-ramjet mode transition Mach number. In fact, without bleed, positive acceleration could not be maintained. Higher fidelity studies with a more optimal vehicle could change the magnitude of the result, but the suggested benefit of liquefied bleed is significant.

During the first 6 months, the efforts were focused using a facility certified for liquid hydrogen experiments. Making a small supersonic wind tunnel was found to be easier than certifying a facility for liquid hydrogen safety. The GRC RCL provides a safe test environment for use of liquid hydrogen. Use of the 1×1 SWT will still be considered but for non-chilled and LN2-cooled bleed experiments. Two cryogenic test cells were being considered: ACS (Figure 5) and SMiRF (Figure 9).

Figure 9. Exterior view of SMiRF, the Small Multipurpose Research Facility.

Under Phase 1 seedling funding, some of the hardware for the liquefied bleed testing were fabricated. The initial hardware can be set up for a simple supersonic flow test without the heat exchanger. This quick test would assess the flow quality of the Mach 3 nozzle/diffuser design. Figure 10 shows this hardware in relation to the design schematic.

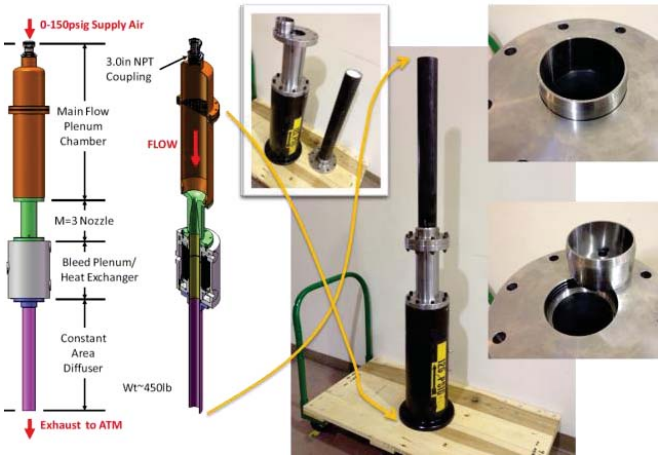

Figure 10. Mach 3 nozzle / diffuser hardware fabricated under the Phase 1 Seedling Fund.

Requirement documents for both tests have been submitted to the GRC facilities personnel for feedback and planning purposes (References 5 and 6). As previously mentioned, the SMiRF facility was chosen to develop rough-order-of-magnitude costs due to its liquid hydrogen capabilities.

The promise for additional support outside of the Seedling Fund is a long-term proposition. High-speed aeronautics was unable to fund GRC for hypersonics for the previous fiscal year, (FY13). The Air Force and NASA are collaborating by funding the next phase of TBCC testing for the current fiscal year. Liquefied bleed technology was discussed with the Air Force Research Lab as a possibility for the far-term plans of TBCC/CCE project.

Future Plans

The rough-order-of-magnitude cost information derived from the test requirements for two distinct tests was ascertained. Each of the two tests would require about twice the available resources through the Phase 2 Seedling Fund. Therefore, the Liquid Bleed (LB) effort will not be proposed for immediate continuation. At a reduced staffing level, the next steps will be: investigation of ways to reduce costs, evaluation of test facilities, investigation of alternate fund sources, and re-scoping of test objectives. The future work will lead to a robust future proposal to continue the LB investigation.

Current TRL: The Technology Readiness Level (TRL) = 2: The technology concept and application are being formulated. POC testing has been identified, designed, and planned.

Applicable NASA Programs/Projects

Benefits of the Liquefied Bleed technology would be applicable to the Fundamental Aeronautics Program/High-Speed Project. A direct application would be for hypersonics research, a project that is currently on hold. A long-term application of the technology may also be for a future fleet of supersonic aircraft that have transitioned to cryogenic methane or hydrogen to reduce carbon emissions.

References

1. Foster, L.E.; Saunders, J.D., Jr.; Sanders, B.W.; Weir, L.J.: "Highlights from a Mach 4 Experimental Demonstration of Inlet Mode Transition for Turbine-Based Combined Cycle Hypersonic Propulsion." 48th Joint Propulsion Conference and Exhibit; 30 Jul. - 1 Aug. 2012; Atlanta, GA, NASA/TM-2012-217724, December 2012.
2. Saunders, J.D.; Foster, L.E.; Sanders, B.W.; Weir, L.J. "Demonstration and Performance of Inlet Mode Transition for Turbine-Based Combined Cycle Hypersonic Propulsion." JANNAF Propulsion Meeting/33rd Airbreathing Propulsion/Joint Subcommittee Meeting; 3-7 Dec. 2012; Monterey, CA; Limited by International Traffic in Arms Regulations (ITAR); NASA/TM-2013-217839, May 2013.
3. McLafferty, G.: Pressure Losses and Flow Coefficients of Slanted Perforations Discharging from within a Simulated Supersonic Inlet. UTRC R-0920-1, Dec. 1958.
4. Schlichting, H., (Kestin, J. transl.): Boundary-Layer Theory, Seventh Edition, Chapter XXIII. McGraw-Hill Book Company, 1979.
5. Davis, D.O; "Liquefied Bleed for Stability and Efficiency of High Speed Inlets: Small-Scale Liquid-Bleed (SSLB) Test Requirements" , Revision 0, Jan. 13, 2014.
6. TechLand Research Inc.; "Liquefied Bleed for Stability and Efficiency of High Speed Inlets: Bleed Cooling Test in the NASA GRC 1x1 SWT Test Requirements", Revision 0, Dec. 2013.
7. Cassidy, M.D.; "Performance Sensitivities of a High Altitude Mach 5 Penetrator Aircraft Concept", NASA CR-3932, 1985.
8. Cubbison, R.W., and Barnett, D.O.; "Performance Characteristics of a Wing-Body Combination with a Two-Dimensional External-Internal-Compression Inlet at Mach 3.5 and 3.0", NASA TM-X-256, July 1960.
9. Hehs, E.: "Super Hustler, FISH, Kingfish, And Beyond: Part 4: Beyond Kingfish", Posted 9 March 2012, http://www.codeonemagazine.com/article.html?item_id=92 , Accessed April 14, 2014.
10. Hill, Phillip G.; and Petersen, Carl R.; Mechanics and Thermodynamics of Propulsion, Addison-Wesley, 1970.

Patents

The technology developed during the Phase 1 funding was proposed for patent activity through a new technology disclosure form.

Nomenclature

1×1 SWT	1- by 1-Foot Supersonic Wind Tunnel
10×10 SWT	10- by 10-Foot Supersonic Wind Tunnel
A_{bleed}	Area of bleed porous holes
A_{inf}	Area of capture stream tube
A_{ref}, A_o	Inlet reference area
A_{spill}	Area of spillage air stream tube
ACS	Altitude Combustion Stand
BL	baseline
CCE LIMX	Combined-Cycle Engine Large Scale Inlet Mode Transition Experiment
C_d	drag coefficient
C_{d0} (or C_{d_0})	zero-lift drag coefficient
C_l	lift coefficient
DMRJ	dual-mode ramjet
DWF	dry weight fraction
f	function
FWF	fuel weight fraction
FY	fiscal year
HEX	heat exchanger
I_{sp}	specific impulse
L/D	lift-to-drag ratio
LB	liquefied bleed
LH2	liquid hydrogen
LN2	liquid nitrogen
LOX	liquid oxygen
lsf	linear scale factor
M	Mach number
M_0, M∞	Freestream Mach number
M_{loc}	Local Mach number
M_{stage}	stage Mach number
$\dot{m}$	mass flow rate
N	number of turbine engines
NIST	National Institute for Standards and Technology
NB	No bleed
P_{bleed}	bleed air plenum pressure
P_{t0} (or P_{t_0})	Freestream total pressure
P_{t1} (or P_{t_1})	Inlet entrance total pressure
P_{t2} (or P_{t_2})	Inlet exit total pressure
POC	proof of concept
PWF	payload weight fraction
q	flight dynamic pressure
RCL	Research Combustion Laboratory
SMiRF	Small Multi-propose Research Facility
SWF	structure weight fraction
$T/\dot{m}_a$	specific thrust, thrust per inlet airflow
T_{bleed}	bleed air temperature
TBCC	Turbine-Based Combined-Cycle
TOGW	take-off gross weight
TRL	Technology Readiness Level
TSTO	Two-Stage-To-Orbit

Appendix A. Thermal Balance Analysis

Introduction

One of the first steps to understand the feasibility of the liquefied bleed (LB) concept is to analyze the thermal balance between the cooling capacity of the cryogenic fuel and the bleed flow in the inlet. A series of assumptions were incorporated into the thermodynamic analysis. Results are presented for a typical bleed region showing the amount of density increase as a function of fuel exit temperature.

Approach

The baseline liquefied bleed system was chosen based on the R1 bleed region in the CCE LIMX inlet, References 1 and 2. This forward bleed region has particularly low bleed plenum pressure. R1 bleed would both benefit greatly from a LB system and provide the greatest challenge to thermal balance because of low pressure within which the heat exchanger would operate. The analysis assumed that the fuel was liquid hydrogen. The hydrogen from the fuel tank would enter the LB heat exchanger at 30 R. This inflow fuel temperature maximizes the cooling capacity. In a real system, the hydrogen would likely enter the heat exchanger at a higher temperature, which would reduce the cooling effect on the bleed air. Future refinement would vary this temperature to understand the upper bound on the inlet temperature.

For the thermal balance analysis, the hydrogen exit temperature is varied from this inlet temperature of 30 to 540 R. At each exit temperature, the hydrogen enthalpy change is computed. Then, the bleed air enthalpy change is computed using an energy balance. Given the final enthalpy of the air and the pressure, the temperature and density can be evaluated.

These thermodynamic properties are evaluated by interpolating NIST (National Institute for Standards and Technology) tables. Dry air density and enthalpy tables were created from the NIST database. Also, para-hydrogen enthalpy tables were created from the NIST database. Hydrogen is assumed to be an equilibrium mixture of para-hydrogen and ortho-hydrogen with different thermodynamic and transport properties. [Equilibrium hydrogen is >99.9% para at 36 R and ~25% para at 540 R. Without a catalyst, para-ortho conversion is slow.]

Conditions for the R1 bleed are given in Table A.1. In the first row, the hydrogen flow used to cool the bleed air was set to 41.67% of stoichiometrically-available hydrogen. The second row is set to use 100% of stoichiometrically-available hydrogen for bleed air flow cooling.

$\dot{m}$, tunnel (lbm/s)	$\dot{m}$, bleed (lbm/s)	$\dot{m}$, hydrogen (lbm/s)	P_{bleed} (psia)	T_{bleed} (R)
1.904	0.2855	0.0231	1.137	530
1.904	0.2855	0.0555	1.137	530

Table A.1. Conditions analyzed for a LB system.

Results

Figure A.1 shows an example of the data compiled from the NIST database for dry air. Note that the triple point pressure for air is 0.91 psia and the triple point temperature is 107.6 R. So the data in the figure are just about the triple point pressure. Below triple point conditions, the phase transition will be from gas directly to solid.

4: air: p = 1.137 psia

	Temperature (°R)	Pressure (psia)	Density (lbm/ft³)	Quality (lbm/lbm)
1	108.0	1.137	59.71	Subcooled
2	109.0	1.137	59.57	Subcooled
3	110.0	1.137	59.43	Subcooled
4	111.0	1.137	59.28	Subcooled
5	111.1	1.137	59.27	0.0000
6	112.0	1.137	0.08248	0.1835
7	113.0	1.137	0.04568	0.3714
8	114.0	1.137	0.03486	0.5438
9	115.0	1.137	0.03008	0.7028
10	116.0	1.137	0.02766	0.8502
11	117.0	1.137	0.02644	0.9873
12	117.1	1.137	0.02636	1.000
13	118.0	1.137	0.02616	Superheated
14	119.0	1.137	0.02593	Superheated
15	120.0	1.137	0.02571	Superheated

Figure A.1: Dry air thermodynamic properties.

Using the dry air and hydrogen properties, the state of the bleed air exiting a heat exchanger can be calculated. In Figures A.2 and A.3, the results of the energy balance calculation are shown. For this analysis, the heat exchanger is assumed to be 100% efficient. Also, the hydrogen entering the heat exchanger at 225 psia is assumed to be supercritical.

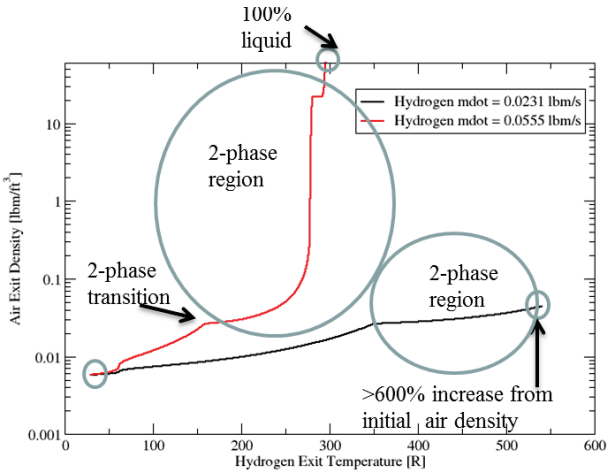

Figure A.2. Results of the thermal energy balance through a liquefying bleed heat exchanger. Air densification as a function of hydrogen exit temperature.

At the nominal hydrogen flow rate (41.67% of the stoichiometric flow), allowing the hydrogen temperature to increase to room temperature results in more than a 600% densification. At the greater flow rate, (100% of the stoichiometric flow), the bleed air can become fully liquefied.

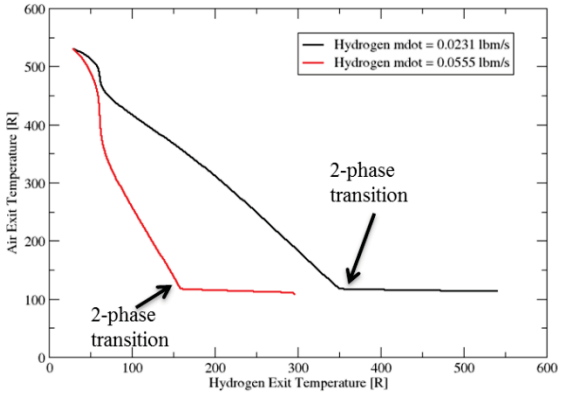

Figure A.3. Results of the thermal energy balance. Air exit temperature as a function of hydrogen exit temperature.

From this nominal analysis, several variations were investigated. These included: variable heat exchanger efficiency, inflow hydrogen pressure, and inflow hydrogen temperature.

The effect of heat exchanger efficiency was investigated by reducing the efficiency by 50%. Results are presented in Figure A.4. Again, the hydrogen is assumed to enter the heat exchanger with supercritical properties at 225 psia.

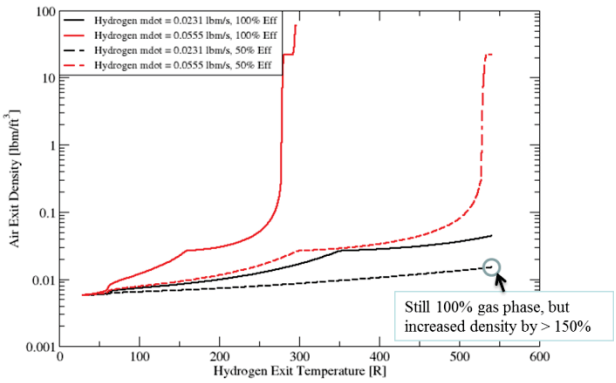

Figure A.4. Results of varying the heat exchanger efficiency on the thermal energy balance. Air density as a function of hydrogen exit temperature.

Heat exchanger efficiency has a significant effect on densification. At 50% efficiency, even at higher hydrogen flow rate, exit air remains in the two-phase region.

Crystallization of water vapor and carbon dioxide is at least one source of inefficiency. Figure A.5 shows the phase diagram for carbon dioxide. At 1 psia, carbon dioxide will start crystallizing at ~300 R and water vapor will start crystallizing at ~452 R. Frost build-up on the heat exchanger increases the thermal resistance, resulting in less heat transferred from the bleed air to the hydrogen.

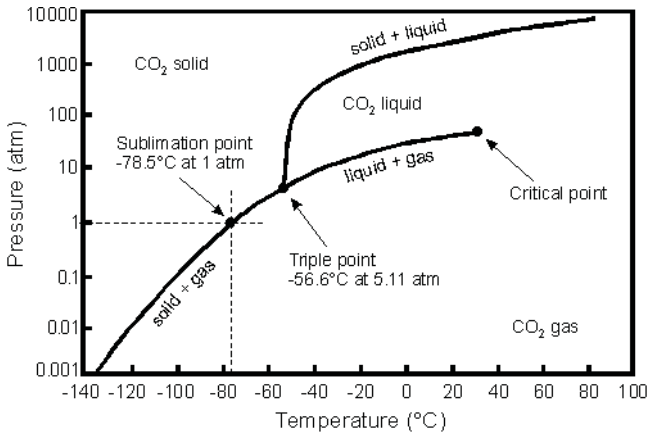

Figure A.5. Results of varying the inflow hydrogen temperature on the thermal energy balance. Air density as a function of hydrogen exit temperature.

The effect of inflow hydrogen pressure was investigated by reducing the pressure from 225 to 40 psia. Results are presented in Figure A.6.

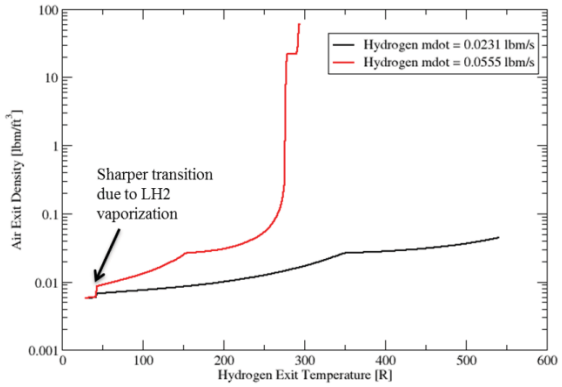

Figure A.6. Results of varying the inflow hydrogen pressure to 40 psi on the thermal energy balance. Air density as a function of hydrogen exit temperature.

Note that the hydrogen enters as a subcritical fluid at 40 psia. This figure, when compared to Figure A.1, shows similar behavior as the supercritical case. This result is not surprising since hydrogen enthalpy is a weak function of pressure.

A final variation was examined by varying inflow hydrogen temperature (Figure A.7).

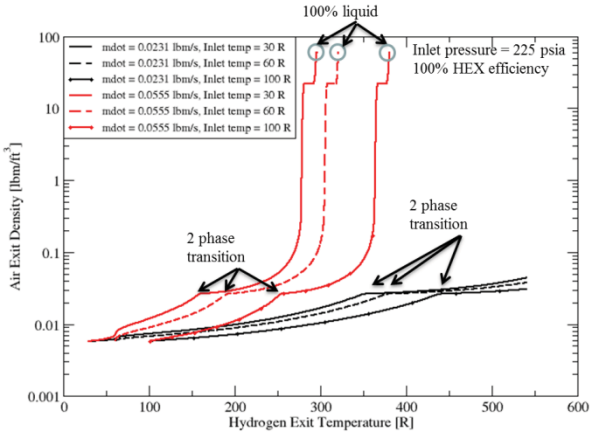

Figure A.7. Results of varying the inflow hydrogen temperature on the thermal energy balance. Air density as a function of hydrogen exit temperature.

Hydrogen will warm as it flows from the supply tank and undergoes compression by the pump. The heat exchanger efficiency is kept at 100% for this analysis. Note that only a small resulting region exists where 100% of the bleed flow is liquefied. There is a large region of conditions where two-phase flow exists. As with the other trends, the density increase is not as large as when it is fully liquefied, but there is a significant increase.

Summary

The data indicate that under ideal conditions, bleed air will begin to liquefy.

For the nominal case (0.0231 lbm/s hydrogen), the air exiting the plenum would be a two-phase mixture of gas and liquid resulting in >600% increase in the air density.

The results are a strong function of the heat exchanger efficiency, and more detailed analysis and testing is required to quantify the inefficiencies. Ice frost from water vapor and carbon dioxide may be one source of this inefficiency.

For this bleed air condition (forward ‘R1’ bleed from the CCE LIMX test) significant densification can occur using the cryogenic fuel. Therefore significant reductions in the bleed ducting volume and bleed drag are feasible.

Appendix B. Mission Analysis Study

Approach

The approach to conducting a mission analysis to assess the liquefied bleed technology was broken down into the following steps:

1. Select mission and vehicle concept
2. Pick relevant assumptions
3. Develop a trajectory analysis tool
4. Conduct trade studies

Mission and Vehicle Concept Selection

The mission selected for this study was the Two-Stage-To-Orbit (TSTO) vehicle to deliver payload to low-earth orbit. This mission is similar to the direction taken by the Fundamental Aeronautics Program/Hypersonic Project and its predecessor project whose funding was terminated in 2012. These projects all used a TSTO vehicle in their goal vision. NASA-funded efforts have generally used hydrogen as a fuel because this allows wider Mach operating ranges than less volatile fuels. The liquid bleed technology applies to the first stage of the TSTO vehicle which uses two airbreathing engines in an 'over/under' configuration.

For take-off to Mach 4 conditions, advanced high-temperature-capable turbine engines would provide the accelerating thrust. Beyond Mach 4, propulsive thrust would transition to a DMRJ. The Mach 4 speed is termed the transition Mach number. The turbine engines are located above the DMRJ duct in a typical vehicle configuration leading to the 'over/under' propulsion scheme depicted in Figure B.1. Because this propulsion system uses turbine engines, it is referred as Turbine-Based-Combined-Cycle (TBCC) propulsion. The transitioning inlet system has been tested and discussed in References 1 and 2. Vehicle system studies which helped to guide this mission analysis are documented in References 7 to 9.

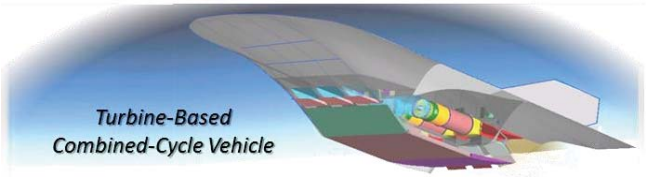

Figure B.1. A Turbine-Based-Combined-Cycle Vehicle with an 'over/under' engine configuration.

The second stage of the vehicle is not addressed explicitly in this study. It could be a pure rocket or a hybrid scramjet rocket with liquid oxygen (LOX) augmentation. This stage would contain the orbital payload and accelerate from the staging Mach number of 7 to orbital speed. The liquid bleed technology may be applicable to a scramjet-based second stage. However, its impact on the overall vehicle is thought to be greater for the first stage. Consequently, the impact of liquid bleed technology on the first stage is the focus of this study.

This study's analyses were held at a low-fidelity level, consistent with this effort's scope and low TRL of the LB concept.

Assumptions

Funding levels limited the amount of detail that could be included in the analysis. Absolute predictions of mission performance were not the goal. Rather, a reasonable baseline was simulated from which relevant sensitivities could be understood. The sensitivity of the baseline mission to liquid bleed technology was the goal.

Many simplifications were assumed. The assumptions made for the analysis of the selected TSTO mission to a staging Mach number are listed below.

1. *Baseline Vehicle Design*
2. *Vehicle Geometry*
3. *CCE LIMX flow splits and performance*
4. *Liquefied bleed densification*
5. *Effects due to liquefied bleed*
6. *Vehicle Dry Weight Fraction*
7. *Trajectory dynamic pressure*
8. *Simplified aerodynamics*
9. *Simplified engine performance*
10. *Trim drag*

They will be discussed individually below. Many of these assumptions are not simple constants or functions. For these assumptions, details of their calculations are modeled within the MSExcel spreadsheet, "Access2Space_v5.xlsx."

1. Baseline Vehicle Design

This simplified analysis utilizes weight fraction analysis as outlined in chapter 10 of Reference 10. Weight fractions are defined for the payload, structure, dry, and fuel (PWF, SWF, DWF and FWF, respectively). The dry weight is the sum of the payload and structure. For the baseline vehicle, the payload was set to 8%, (PWF = 0.08). For the first stage, this 'payload' is the entire second stage. The structural weight fraction was optimistically set to 42%, (SWF = 0.42), so the dry weight fraction is 50%, (DWF = 50%). Note that the SWF include the 'payload' of the second stage. The remaining weight, 50% of the TOGW, is available for fuel, (FWF = 0.5), or 1 million pounds for our baseline vehicle.

The design parameters for the vehicle were chosen based on experience with an eye to avoid overly constrained or non-linear areas of the mission space. In other words, the vehicle design is intentionally non-optimal to allow easier sensitivity analyses. Some of specific elements are listed below:

- 0.5 is the baseline dry mass ratio or dry weight fraction, (DWF)
- Second stage (payload) mass ratio is part of the first stage's DWF

- 2.0 million pounds is take-off gross weight
- 0.663 is thrust ratio (thrust/weight)
- 9 is the number of turbine engines, (N)
- 0.23 is turbine engine frontal-area ratio
- 2800 is the frontal area at zero lift, ($ft.^2$)
- 0.05 is the zero-lift drag coef.
- 0.12 is the wing thickness-to-chord ratio
- Vehicle is not volume constrained

2. Vehicle Geometry

As mentioned above, the baseline vehicle size was assumed to be 2 million pounds. TOGW was variable as a function of staging Mach number. By holding the stage Mach number to 7, the effect of trades such as implementing liquid bleed technology could be determined. The relative sizing of the vehicle elements (i.e., propulsion to wing to volume) was held constant per linear geometric scaling.

From these assumed design parameters, the following vehicle size elements were calculated:

- 333.8 wing span (ft.)
- 90.422 wing chord (ft.)
- 10.851 thickness (ft.)
- 3621.5 wing area ($ft.^2$)
- 2800.0 body area ($ft.^2$)
- 30,180 wing reference area, ($ft.^2$), including area submerged within the fuselage
- 59.71 body diam. (ft.)
- 0.9811 lift coef. at take off
- 3.691 wing aspect ratio
- 114.54 turbine engine dia., (in.)
- 1202.2 propulsion frontal area, ($ft.^2$)
- 48.68 width turbine stack [N+1/N-1], (ft.)

Note that these large dimensions reflect the non-optimal take-off gross weight of 2 million pounds. These geometric sizes were used to develop a crude sketch of the vehicle, which is shown in Figure B.2.

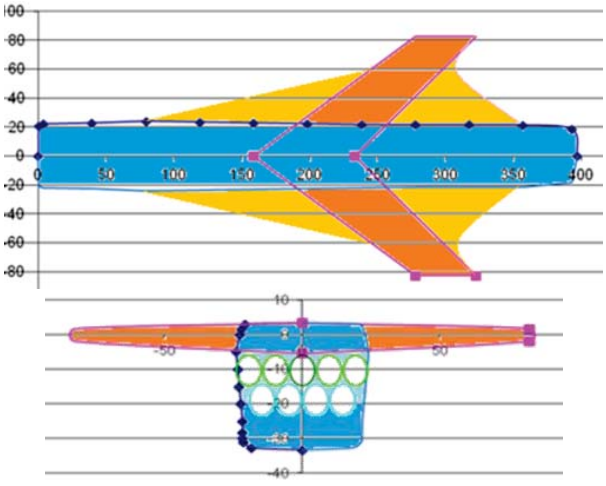

Figure B.2 Vehicle sketch representing design parameters guiding the mission analysis (dimensions in feet).

3. CCE LIMX flow splits and performance

The inlet is characterized by recovery and flow ratios as a function of flight Mach number. As mentioned, the flow splits and performance for the vehicle's inlet system are documented in Reference 2. Flow capture and spillage are derived from the CCE LIMX testing. Figure B.3 shows the inlet capture versus flight Mach number for both the turbine and scramjet engines. Also shown are the engine entrance (or inlet exit) Mach numbers used to design the inlet.

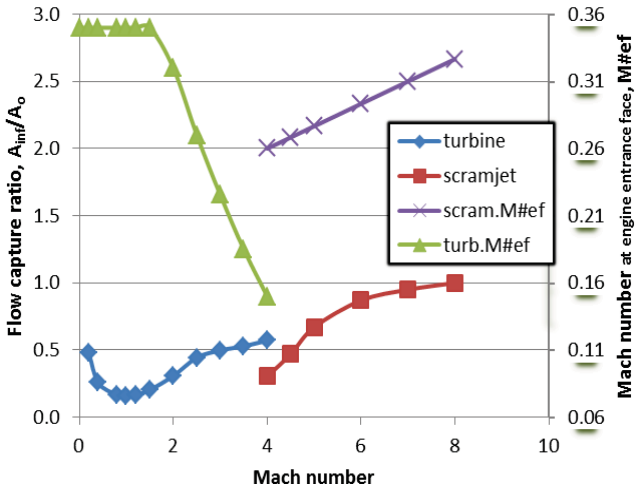

Figure B.3 Flow capture ratios and engine face Mach numbers derived from CCE LIMX design.

The following curve (Figure B.4) shows the explicit flow spillage ratio numbers as well as bleed-flow ratios. The indicated curvefits were used to represent the flow changes in the simulation as Mach number increases. For the configurations that include bleed, the bleed flow was increased 30% to total 130% of the rates shown in Figure B.4. Above Mach 4, the bleed was held constant at the Mach 4 level for the liquefied bleed option. This implies that bleed is used by the DMRJ flow path.

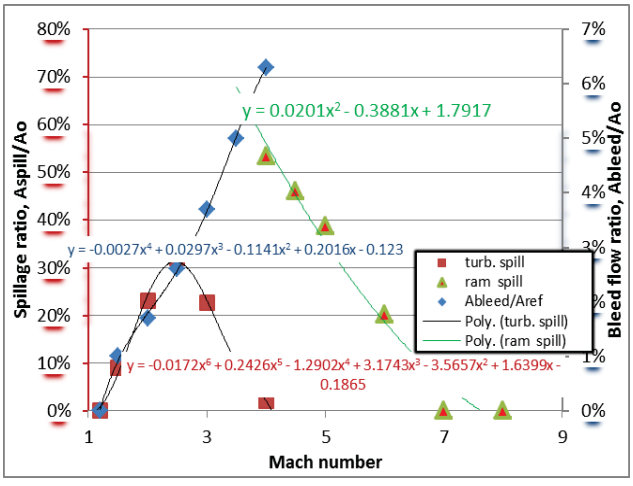

Figure B.4 Flow capture ratios and engine face Mach numbers derived from CCE LIMX design.

Figure B.5 shows the MIL-E-5007D specification for inlet total pressure recovery.

$P_{t2}(ref)/P_{t_0}$ = 1.0 From Zero to 1.0 Mach Number

$P_{t2}(ref)/P_{t_0} = 1.0 - 0.075(Mo - 1)^{1.35}$ From 1.0 to 5.0 Mach Number

MIL-E-5007D

$P_{t2}(ref)/P_{t0} = \frac{800}{M_0^4 + 935}$ Above 5.0 Mach Number

Figure B.5 Mil-spec equations defining inlet pressure recovery as a function of Mach number.

Recovery is based on 90% of mil-spec for a high performance inlet with bleed. Figure B.6 shows the total pressure recovery versus Mach for a bled inlet (indicating use of liquid bleed technology). Without bleed, the recovery for the inlet might be as low as 1/4th (25%) of the bled inlet recovery. With the baseline vehicle size, the vehicle net thrust became zero around Mach 2 at 36% of the bled recovery. Therefore, only a reduction to the 37.5% level was assumed to allow the mission analysis to progress through Mach 4 mode transition. This level of recovery may require performance beyond a realistic 'No Bleed' inlet. In truth, this low level of recovery would require vehicle redesign with proportionately larger turbine and scramjet inlets to avoid intermediate Mach number 'pinch' points.

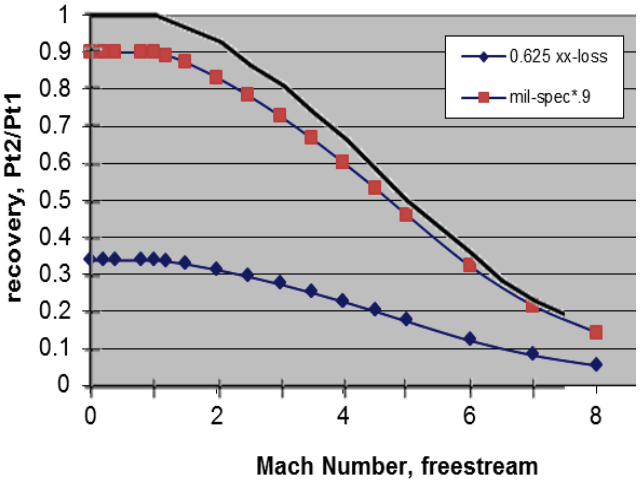

Figure B.6 Mil-spec inlet pressure recovery and the assumed baseline recovery for a bled inlet (90%) and for an unbled inlet (37.5%).

4. Liquefied bleed densification

Using TBCC mode transition inlet design, a range of bleed flow rates and fluid states were used to size the heat exchanger and facility equipment. From this bleed environment, the thermodynamic effect of cryogenic cooling was analyzed to see how much the air density could be increased and to what degree liquefaction is possible (detailed in Appendix A). In Figure B.7, plots of the bleed air's possible exit conditions as a function of hydrogen exit conditions are shown. In both cases, supercritical hydrogen is entering the heat exchanger at 225 psia and 36 R.

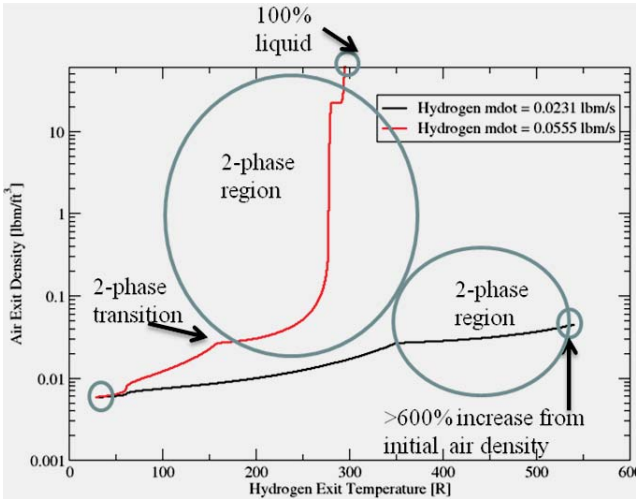

Figure B.7. Bleed air exit conditions.

At a moderate LH2 flow rate, more than a 600% increase in bleed air density may be expected. If the hydrogen-to-bleed air ratio is more aggressive, complete air liquefaction is possible. These results support concept feasibility. Heat exchanger sizing and design is underway and detailed test planning has begun.

5. Effects due to liquefied bleed

Taking full benefit of the liquid bleed technology, the bleed drag was assumed to be zero. Trades were examined in which the bleed drag occurs 1) without cooling for the baseline configuration and 2) without bleed in the inlets. Future analysis could examine the benefit with partial cooling or densification of the bleed air stream.

6. Vehicle Dry Weight Fraction

A critical variable in the trade studies turned out to be the vehicle's dry weight fraction. A lesson learned was that the DWF is not an independent variable to TOGW. As the vehicle gets smaller, the DWF tends to increase due to scaling laws (linear, areal, and volumetric). Finding the scaling law functionality is the key to improving mission analysis fidelity. For this study, a simplistic approach was taken to get approximately correct effects. The effect of the trades is delta effects from the baseline. Absolute values in this analysis are not valid; for example, the baseline vehicle weight of 2 million pounds was set arbitrarily. Therefore, a vehicle weight reduction due to liquid bleed is only approximately true as relative (percentage) change that is affected by the validity of the scaling law assumption as well as the other assumptions. The variation in DWF is

discussed in more detail in the next section on the trajectory analysis tool.

7. Trajectory dynamic pressure

Choosing a 'best' flight dynamic pressure is difficult. It involves a conflicting trend between structures and aeropropulsion efficiency. The trajectory of accelerating flight is usually targeted at a certain flight dynamic pressure, q. The dynamic pressure scales wing aerodynamics, flight angle of attack, propulsion efficiency, and vehicle structures. Optimization requires higher fidelity design than in this analysis. Instead, a simplified assumption was made to fly the vehicle along a nominally constant-q trajectory. For long-range cruise vehicles, the typical flight q ranges from 400 to 700 psf. For highly maneuverable or accelerating vehicles, flight q might be increased to 1000 or even 2000 psf. However, higher pressure loads begin to drive structural weight fractions in this range of dynamic pressure. The relationship can become non-linear and 'mission-destroying'. For this reason, a less aggressive flight q of 1000 psf was chosen. The propulsion aspect of choosing a flight q becomes critical if engine ignition and flameout become problems due to low pressures. At 1000 psf and with a volatile fuel like hydrogen, ignition and flameholding—while challenging—should not be a show-stopper.

8. Simplified aerodynamics

The aerodynamics properties of this study vehicle are simplified; they are restricted to Mach number and angle of attack functionality. From a sizing spreadsheet, wing planform areas and vehicle frontal areas are estimated. Zero-lift drag curves as a function of Mach number for a non-lifting body are incorporated (Figure B.8).

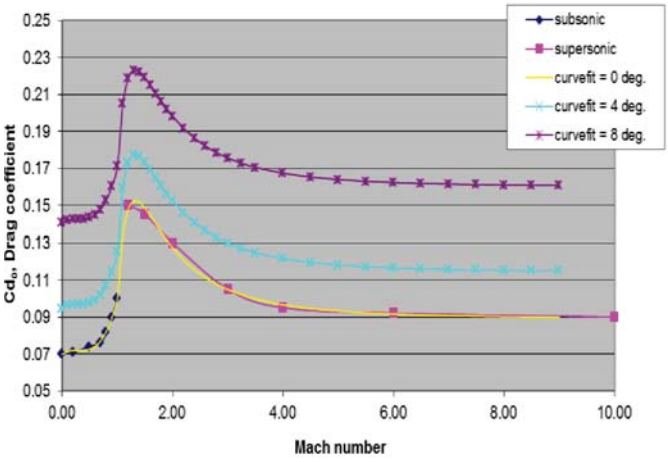

Figure B.8. Effect of Mach number on zero-lift drag coefficient.

The effect of angle-of-attack on drag is also added. The lift due to the wing is estimated based on finite wing subsonic theory. Lift is degraded when the angle of attack approaches 15°. No correction is made to lift due to Mach. Drag due to lift is added to the zero-lift drag. Drag polars are constructed and appear to be reasonable for a low-fidelity mission analysis (Figure B.9). Lift-to-drag ratios (L/D) at supersonic and hypersonic Mach numbers for the present study are low (conservative) relative to cruise vehicles discussed in References 7 to 9. The L/D levels were in the range of 1 to 2 for the higher Mach numbers, (not shown). However, some L/D reduction would be expected for this LH2 fueled system due to hydrogen's volumetric penalty, (the low density of LH2 results in large, bulky fuel tanks dominating the vehicle design).

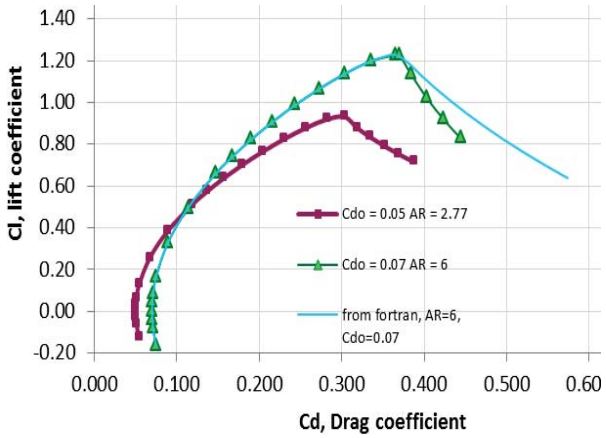

Figure B.9. Drag polars with simple stall model.

9. Simplified engine performance

The details of the propulsion modeling are the most complicated aspect of the assumptions. The inlet modeling was discussed under assumption 2, above. The engine modeling is based on concepts from Reference 7. The engine was characterized by fuel efficiency, (specific impulse, I_{sp}) and specific thrust, ($T/\dot{m}_a$) as functions of Mach number. Fuel is erroneously assumed to be a hydrocarbon. For liquid bleed, the fuel should have been cryogenic hydrogen. This error affects the fuel efficiency, but should not affect the trade study between the 'no bleed' and 'liquid bleed' vehicle. The fuel effect on fueling efficiency should be corrected in future studies—a simple correction would be to multiply the I_{sp} by the stoichiometric fuel/air ratio, 2.34 = [6.8%/2.9%]. The effect of fuel type on $T/\dot{m}_a$ is less straight-forward as it depends on whether the higher stoichiometric combustion temperature for hydrogen can be maintained in a practical engine.

Figure B.10 shows the assumed I_{sp} and $T/\dot{m}_a$ curves for the turbine engine.

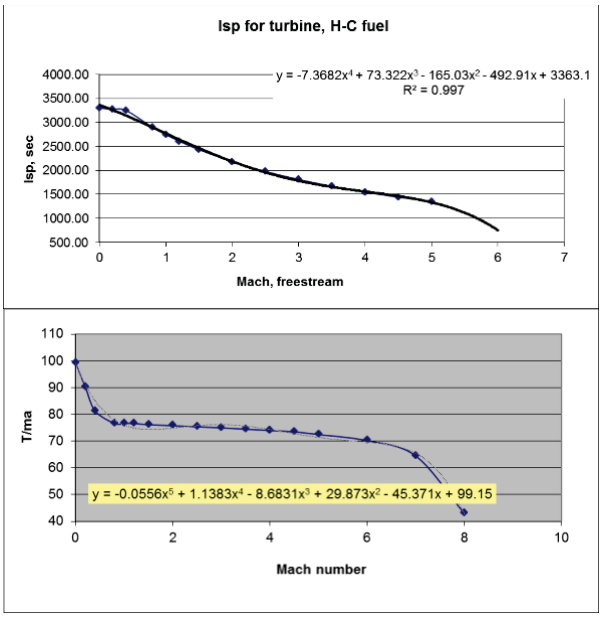

Figure B.10. Modeled turbine engine performance.

Similarly, the assumed $\boldsymbol{I_{sp}}$ and $T/\dot{m}_a$ curves for the scramjet, or 'afterburning' curves, are shown in Figure B.11. This scramjet performance is pessimistic. In fact, above Mach 8, the $T/\dot{m}_a$ and $\boldsymbol{I_{sp}}$ are held constant at the Mach 8 levels. With this assumed scramjet performance, acceleration beyond Mach 8 becomes increasingly difficult.

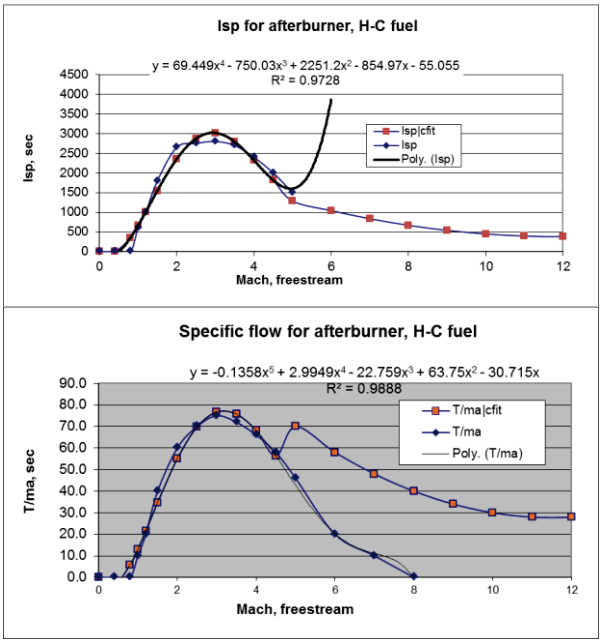

Figure B.11. Modeled scramjet engine performance.

Since the TSTO vehicle is designed for an acceleration mission, engine performance is simplified by assuming both the turbine and DMRJ engine operate near maximum fuel flow or maximum material temperature limits.

Modeling different throttle positions for the engines has been considered but has not been implemented in detail. However, for the turbine engine, reduced inlet total pressure would require reduced corrected flow or a new inlet system. Within the scope of this study, the inlet relative size and design were held constant. Reduced recovery was therefore treated by linearly reducing specific thrust. Specific impulse was held constant.

10. Trim drag

Trim drag is not addressed explicitly. It is assumed to be part of the overall drag force, which itself, reflects a low-fidelity approximation. Therefore, the angle-of-attack is assumed to change slowly so that trim drag is not a major and variable component of the overall drag.

Trajectory analysis tool

Towards the end of funding for the Aeronautics Research Mission Directorate's Fundamental Aeronautics Program/Hypersonics project, a low-level effort was made to understand the impact of airbreathing propulsion on the access-to-space mission. Development of a FORTRAN-based simulation of a representative TBCC mission was begun. (The effort was initially targeted to use a tool based on Microsoft Excel, but limited iteration capability in Excel drove the trajectory analysis into a traditional programming language. The author was familiar with FORTRAN instead of Excel's VisualBasic). This code was refined and checked under the Phase 1 funding of the LB project. Inputs to the code were adjusted to reflect the mission assumptions and then to capture the first-order effects of a liquefied bleed system. The FORTRAN source code is in the file "tbcctraj_v8.for."

One important aspect of the simplified analysis was the powerful effect of dry weight fraction on mission performance. Initially, the baseline DWF of 50% was held constant. However, unexpected results occurred when vehicle parameters were varied. Reflecting on these results and in consultation with mission analysis experts, the assumption of constant DWF was realized to be deeply flawed. As a vehicle shrinks in size, the engines and structure do not shrink as much as the fuel/payload capacity. Fundamentally, this is due to first-order scaling laws: structure tends to scale linearly with geometric size. Propulsion might scale to a power of 2 or more. Also, fuel capacity scales volumetrically with a power of 3. Because of these strong scaling law effects, the DWF must increase as the vehicle size is reduced.

The final correlation between DWF and TOGW was derived in the Excel spreadsheet, "DWF(TOGW)_v3." The resulting correlation that was initially used in the trajectory analysis is shown in Figure B.11.

In mathematical detail, this correlation was fit to an exponential/logarithmic relationship so that reduced DWF could be found from TOGW and vice versa. The DWF was further assumed to be composed of an equal split between

propulsion and structure/payload. Therefore the propulsion weight fraction (PWF) was 0.08 and the structural weight fraction (SWF) was 0.42. The fuel weight fraction is simply: FWF = (1 – DWF). The correlation is based on linear, propulsive, and volumetric scale factors. The power factors are 1, 2.3, and 3, respectively. The propulsive scale factor is a mixture between areal (power of 2) and volume (power of 3). From these scaling factors, a new TOGW is calculated as follows:

$$TOGW_{new} = TOGW_{old} * (lsf^{2.3} * PWF + lsf * SWF) + lsf^{3} * (1 - DWF)$$

Finally, a new DWF is calculated as a function of linear scale factor, lsf, as follows:

$$DWF_{new} = \frac{(lsf^{2.3} * PWF + lsf * SWF)}{(lsf^{2.3} * PWF + lsf * SWF) + lsf^{3} * (1 - DWF)}$$

The new values for TOGW and DWF are cross plotted in Figure B.12 to find exponential curvefits to directly relate the two parameters. This correlation holds only for vehicles that are geometrically scaled.

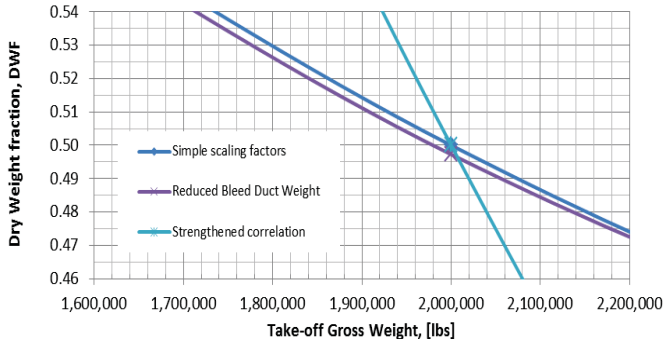

Figure B.12. Negative correlation between TOGW and DWF.

When the vehicles are changed because of system performance enhancements, the TOGW/DWF correlation is also changed. So for the present study, the incorporation of bleed and liquid bleed system change this correlation. Rather than find a complex effect of bleed changes on the TOGW/DWF correlation, the following simplified adjustment was made. For this vehicle/mission, the volume is not physically constrained. This contrasts with a missile application where the vehicle might have to fit under a wing or in a launch tube. Therefore, the effect of the liquefied bleed would be in the weight savings of eliminating the weight of the bleed ducts. Using various liberal assumptions, the weight savings was found to reduce DWF by only 0.00237. This change is small relative to the refinement of the assumptions and accuracy of the analysis. The DWF reduction was not used in the trajectory analysis. However, in a more volume constrained vehicle, this benefit should not be neglected.

Unfortunately, the analysis described in this section only showed how to couple DWF to TOGW qualitatively. When the vehicle/mission trajectories were analyzed, further adjustments were required. These adjustments are discussed in the next section.

Trade Studies with Trajectory Analysis

The space-access mission, which was modeled, simulates an airbreathing TBCC-propelled first stage that could boost a second stage to a staging Mach number of 7. For the first stage, the merit of a liquefied bleed system was assessed by assigning appropriate performance, weight fraction factors, and assumptions to find the resulting minimum TOGW. The LB benefits are increased supersonic inlet recovery, reduced bleed drag and reduced volume. The volume change accommodates a larger fuel fraction. However, the change had a small effect on the weight fractions (discussed later) and was not incorporated into the present analysis. For the preliminary analysis, the liquefied bleed air was assumed to be fully liquefied but then simply vented overboard. No advantage was taken for scramjet or rocket augmentation later in the mission. Therefore, the complexity (and impact) of liquefied bleed-air storage was not modeled. Thermal balance issues between the combustor-wall cooling and the LB system were not assessed in this simplified analysis, either. As mentioned, the TBCC aircraft was not optimized and had a very large TOGW of 2×10^6 lbs.

For the current analysis, three configurations were examined: 1) Baseline with typical high-performance inlet bleed for the turbine flow path, termed "BL." 2) A low-performance "No Bleed" inlet operating without bleed, termed "NB." 3) A high-performance inlet with liquefied bleed, termed "LB." Figure B.13 shows how the amount of bleed or recovery loss affect the final Mach number achieved for the first stage. Initially, in each case, the trajectory analysis program was used, assuming constant levels for DWF equal to 0.5, TOGW equal to 2 million pounds, and flight dynamic pressure q equal to 1000 psf.

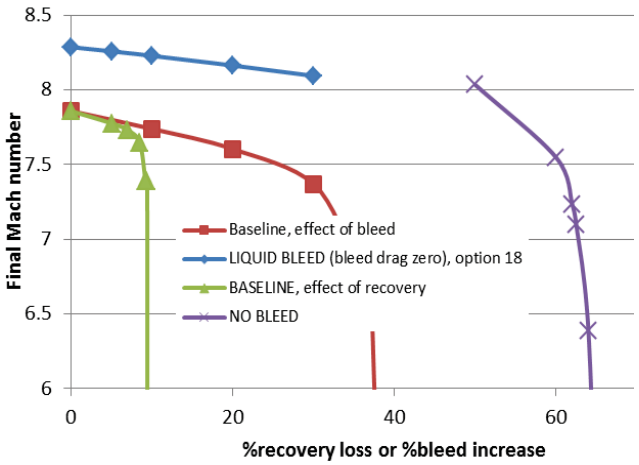

Figure B.13. Results from mission analysis showing the effect of bleed and recovery loss for the three bleed configurations.

Recall that the final Mach for the first stage is targeted for Mach 7. From these trade results, appropriate levels of bleed and recovery loss were selected for each of the three configurations. Ultimately, a mission analysis goal would

be to find the effect of a technology on vehicle total operating cost. The cost is a very complex calculation, but has been found to roughly correlate with the TOGW. Technology with good payoff would reduce TOGW (and cost). To calculate the effect of liquid bleed on TOGW turned out to be more difficult than anticipated. Resizing a vehicle is a very non-trivial, non-linear process. Initially, trajectory analyses were calculated holding the DWF constant.

As mentioned in the prior sub-section, DWF cannot be constant. The chosen negative correlation between TOGW and DWF was put into the trajectory analysis code. Although this scaling helped to correct the improper effect of TOGW on performance, the performance still grew with TOGW reduction. Somewhat arbitrarily, the strength of the negative correlation was increased for DWF = f (TOGW) from a slope –0.132 to –0.446 per million pounds or nearly 3.4 times; this correlation is also plotted in Figure B.12.

The trajectory analysis was then examined for each of the configurations (BL, NB, LB). When this strengthened correlation was used in the trajectory analysis, the appropriate reduction in performance occurred as the TOGW is reduced from the baseline of 2 million pounds. Figure B.14 shows a result from this analysis.

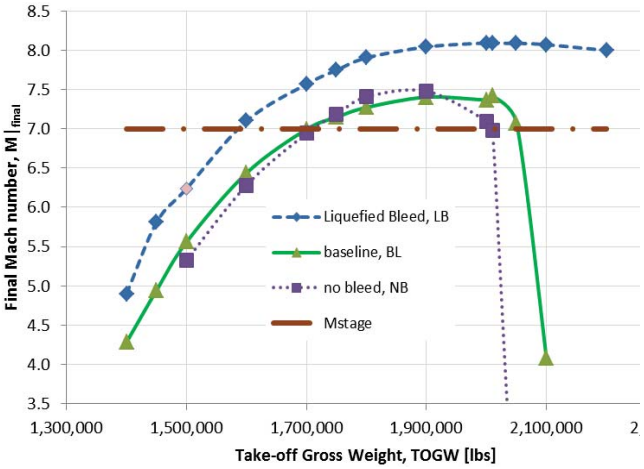

Figure B.14. Results from mission analysis showing a 7% to 23% reduction in TOGW is possible because of liquefied bleed.

This plot indicates that liquefied bleed could reduce TOGW by about 7 to 23%, which is somewhat less than the preliminary number of 30% that was indicated in the final Phase 1 presentation charts. The difference is due to revisiting the analysis to make refinements and correct errors. The reduced TOGW benefit was accentuated by a pinch point at the turbine-to-ramjet mode transition Mach number. In fact, without bleed, positive acceleration could not be maintained when the full decrement in recovery of 75% was used. Therefore, a 62.5% recovery reduction was used; that is, "no bleed" recovery was 37.5% of the bleed recovery.

Examining Figure B.14 more closely, the baseline and no-bleed configurations exhibit an unexpected 'optimum.' Possibly, the higher TOGW caused pinched points at the mode transition Mach number of 4 and/or through the transonic speeds. Also, surprisingly, the no-bleed configuration had a similar performance characteristic to the high-performance bled inlet used in the baseline configuration. The result indicates that the effect of bleed drag versus low inlet recovery can be nearly equivalent. However, note that the full decrement in recovery for the unbled inlet could not be taken. In fact, for the full 75% recovery reduction, the final Mach number was only 1.859, which would indicate a pinch point through transonic speeds.

Note that both the baseline and no-bleed configurations have two solutions for meeting the stage Mach number, M_{stage} = 7. Using the upper number around TOGW = 2.05×10^6 lbs., and the liquefied bleed solution of TOGW = 1.58×10^6 lbs., a 23% reduction in TOGW is indicated. Using the lower weight solutions for both the baseline and no-bleed configuration (TOGW = 1.7×10^6 lbs), a 7% reduction is possible.

With the important caveat that higher fidelity studies with optimal vehicle sizing could change the magnitude of the result, this simplified mission analysis has suggested a benefit of liquefied bleed that is significant.

Summary

A mission analysis code was developed to perform a trade study on the effectiveness of liquefying bleed for the inlet of the first stage of a TSTO vehicle. By liquefying bleed, the vehicle weight (TOGW) could be reduced by 7 to 23%.

Numerous simplifying assumptions were made and lessons were learned. Increased accuracy in future analyses can be achieved by:

- Including a higher fidelity model to capture the effect of rescaling (variable vehicle TOGW)
- Refining specific thrust and impulse models ($T/\dot{m}_a$ and I_{sp}) to preserve fuel-to-air ratio
- Implementing LH2 for $T/\dot{m}_a$ and I_{sp}
- Correlating baseline design to other mission analyses and correcting vehicle design elements
- Implementing angle-of-attack effects on inlet characteristics
- Refining aerodynamic performance (to improve L/D ratio at higher Mach numbers).
- Examining the benefit with partial cooling or densification of the bleed air stream.
- Incorporating higher fidelity weight estimates for the liquefied bleed system (heat exchange and liquid storage versus bleed duct weights) could be added when more fully developed.
- Adding trim drag or 6-degree-of-freedom trajectory analysis for higher fidelity.
- Investigating vehicle optimization for each of the bleed configurations.